A simulation study of the soft and hard radiations using jets at the LHC

R F Haroon[1] and D Roy[2]
[1,2]Amity University, Amity Rd, Sector 125, Noida, Uttar Pradesh 201301, India

[1]raseebharoon@gmail.com and [2]droy@amity.edu

Abstract. In this work, different aspects of the high-energy radiation are looked at considering the LHC scenario. An event-shape variable and several jet substructure observables are studied with the Mote Carlo event simulators at the 13 TeV center of mass energy scale to mimic the current LHC environment. The event-shape and the jet substructure observables are chosen such that they are not only sensitive to the different aspects of the high energy radiation measurement but also exhibit promising features to distinguish the possible existence of new physics that considers a dark matter candidate decaying into semi-visible jet. It is verified that the observables exhibit significant sensitivities to disentangle two jets to multi-jet radiations, presence of a final state and initial state radiations, presence of a large amount of missing transverse energy as a strong indication of the possible existence of a dark matter as well as couple of promising features of a semi-visible jet are explored.

1. Introduction

Large Hadron Collider(LHC) [1] is the world's largest particle accelerator. It delivers the highest energy for particles' acceleration and their collisions that results in the smashing of the counter-rotating proton-proton beams to generate millions of particles. This can result into achieving what may have happened at the instance of the Big Bang. The European Organization for Nuclear Research (CERN) operates this complex series of accelerators to boost various particles to the highest energies ever accomplished by any experiment. The basic process involves accelerating particles in stages, accelerators use different techniques to accelerate particles, such as electric and magnetic fields, and they are synchronized to work together to gradually increase the energy of the particles, with each stage surpassing the energy of the last. The first stage of acceleration is performed by a Linear Accelerator 4 (Linac4), which uses an electric field to accelerate particles to 160 MeV. The Linac4 is followed by a circular accelerator called a Proton Synchrotron Booster, which further increases the energy of the particles by using magnetic fields to accelerate and guide them in a circular path to 2 GeV. Then the Proton Synchrotron boosts the particles to an energy of 26 GeV. After this, the Super Proton Synchrotron accelerates particles to an energy of 450 GeV. The final stage of acceleration is performed by the LHC, a 27-kilometer-long circular tunnel located 100 meters underground, and it is designed to accelerate particles to even higher energies than the Super Proton Synchrotron. The LHC accelerates protons to an energy of 6.8 TeV, allowing them to collide at a total energy of 13.6 TeV. At these energies, particles release energies in terms of radiations namely known as Initial State Radiation (ISR) and Final State Radiation (FSR), before and after the collisions respectively.

In this paper, different types of radiations are studied by simulating the events at the LHC energy scale. Additionally, the generation of the strong radiation, ISR and FSR are also looked at when a possible production of a dark matter candidate is considered through the LHC collisions. In that case,

Content from this work may be used under the terms of the Creative Commons Attribution 3.0 licence. Any further distribution of this work must maintain attribution to the author(s) and the title of the work, journal citation and DOI.
Published under licence by IOP Publishing Ltd

the radiations generated by the presence of the dark matter candidate is studied by utilizing the interplay between the radiations initiated by the conventional matter particles and the dark matter. If the dark matter particle is produced in these collisions, a significant fraction of its radiation evade the detection and takes away the corresponding energy and momentum undetected, causing an imbalance in the observed parameters. Therefore to look for the evidence of a dark matter production, the energy imbalances called the Missing Transverse Energy (MET) is studied and it is compared with the predictions based on the known physics theory [2].

To probe different types of radiations, various jet observables are studied. Jets are particle streams created when a high-energy particle unleashes a stream of new particles. These collimated streams are utilized to study the sensitivity of different types of radiations generated at different stages of their productions. Moreover, they are crucial to distinguish the properties of the particles from which the jets are initiated. At higher and higher energies that the LHC aims to work at, large amounts of these streams of particles are being created, and thus an ever-increasing number of jets are getting produced. Therefore LHC is known as the "Jet Factory." To tap into the potential of this flurry of particles, physicists use jet observables. These are mathematical tools that when applied to a certain environment can give a plethora of information about the physical structure, or properties including but not limited to energy, particles, or angular distribution of final state radiations. Thus, providing insight into the underlying physics processes and enabling a deeper understanding of the behaviors of the particles and the corresponding radiations produced in the high-energy collisions.

2. Jet Observables

Investigating the behavior of a hard radiation produced in high-energy collisions is a critical aspect of high-energy research. Each event at the LHC creates a tremendous amount of data. And sifting through it in a meaningful manner to get results that appeal to our understanding, can be tedious. For this, scientists have devised variables that can give constructive insights into these complex processes. Such powerful tools are known as Jet observables. Experimental measurements of jet observables have been demonstrated to be effective in distinguishing between different types of jets and sensitive to underlying physics processes. Theoretical research has been carried out to provide new algorithms and methods for properly computing these observables. The versatility and use of these observables cannot be understated in high-energy physics.

2.1. Jet event-shape variable

2.1.1. Transverse Thrust(τ_T). One of the most widely used event-shape observable is the transverse thrust [3]. It is used to characterize the geometry of the energy flow. Thrust is defined by a simple mathematical equation,

$$\tau_T \equiv 1 - \max_{\hat{n}_T} \frac{\sum i \ |\vec{p}_{Ti} \, . \, \hat{n}_T|}{\sum i \ \vec{p}_{\mathrm{Ti}}}$$

$\hat{n}_T$ is the unit vector along which the energy thrust is maximum.

2.2. Jet Substructure Variable

2.2.1. Les Houches Angularity ($\lambda^{\kappa}_{\beta^{LHA}}$). Les Houches Angularity (LHA) is the infrared-safe version, with κ = 1, β^{LHA}= 0.5, of the jet-shape angularity used to measure the broadness or amount of hard radiation in a jet. The generalized angularities are expressed as,

$$\lambda^{\kappa}_{\beta^{\mathrm{LHA}}} = \sum_{i \in J} z_i^{\kappa} \, \theta_i^{\beta^{\mathrm{LHA}}},$$

Where θ_i is the i^{th} constituent's angle to the jet axis, normalized by the jet radius, and z_i is the i^{th} constituent's transverse momentum as a fraction of the scalar sum of the p_T of all the components.

2.2.2. Energy Correlation Function(C_2).

$$\begin{aligned} ECF1 &= \sum_{i \in J} p_{T_i}, \\ ECF2(\beta^{ECF}) &= \sum_{i<j \in J} p_{T_i} p_{T_j} \left(\Delta R_{ij}\right)^{\beta^{ECF}}, \\ ECF3(\beta^{ECF}) &= \sum_{i<j<k \in J} p_{T_i} p_{T_j} p_{T_k} \left(\Delta R_{ij} \Delta R_{ik} \Delta R_{jk}\right)^{\beta^{ECF}}, \end{aligned}$$

Which in short can be written as,

$$\begin{aligned} e_2 &= \frac{ECF2}{(ECF1)^2}, \\ e_3 &= \frac{ECF3}{(ECF1)^3}, \end{aligned}$$

Giving us,

$$C_2 = \frac{e_3}{(e_2)^2},$$

β^{ECF} is to be used for weighting purposes, and we use the value $\beta^{\mathrm{ECF}} = 1$ for simplicity. Here i is the constituent of the jet (J). C_2 [4] is sensitive to two prong substructures where each prong can be thought of as a hard radiation source..

2.2.3. N-Subjettiness (τ_{nn-1}). It is a useful identifier to distinguish jets with more prong substructures as compared to a single one. Following are the 0,1,2,3-Subjettiness:

$$\begin{aligned} \tau_0(\beta^{NS}) &= \sum_{i \in J} p_{T_i} R^{\beta^{NS}}, \\ \tau_1(\beta^{NS}) &= \frac{1}{\tau_0(\beta^{NS})} \sum_{i \in J} p_{T_i} \Delta R_{a_1,i}^{\beta^{NS}}, \\ \tau_2(\beta^{NS}) &= \frac{1}{\tau_0(\beta^{NS})} \sum_{i \in J} p_{T_i} \min\left(\Delta R_{a_1,i}^{\beta^{NS}}, \Delta R_{a_2,i}^{\beta^{NS}}\right), \\ \tau_3(\beta^{NS}) &= \frac{1}{\tau_0(\beta^{NS})} \sum_{i \in J} p_{T_i} \min\left(\Delta R_{a_1,i}^{\beta^{NS}}, \Delta R_{a_2,i}^{\beta^{NS}} \Delta R_{a_3,i}^{\beta^{NS}}\right), \end{aligned}$$

Where R is the measure of angular separation in the LHC coordinate system. i is the jet constituent and a_i is the jet axis, and $\Delta R_{a,n}$ is the minimum angular separation between the jet axis and its n^{th} sub jet. β^{NS} is the variable used to get the R variable weighted differently.

The function which is the ratio of two N-subjettiness τ_{nn-1},

$$\tau_{21} = \tau_2/\tau_1,$$
$$\tau_{32} = \tau_3/\tau_2,$$

In our case using $\beta^{NS} = 1$ makes them used to identify jets with two prong and three prong substructures within a jet.

2.2.4. Jet Mass. Tells us about the invariant mass of a jet.

3. Different Radiation in Jet Formation

3.1. ISR

Initial State Radiation refers to the emission of additional radiation by the incoming particles in high-energy particle collisions. In the case of proton-proton collisions at the LHC, the incoming protons are made up of quarks and gluons that can emit additional radiation before the actual proton-proton collision occurs. This other radiation can carry away energy and momentum from the incoming protons, which can affect the properties of the final state of radiation produced in the collision.

Where the reduction in effective center-of-mass energy available for the hard scattering process is one of the fundamental impacts of ISR. This is since the emission of ISR might reduce the velocity of the incoming protons, reducing the available energy for the actual proton-proton collision. This effect is especially relevant at the LHC, where collisions occur at extremely high energies, and the quantity of accessible energy can have a significant impact on the characteristics of the final state of the radiation. ISR is an essential factor to consider in high-energy particle collisions because it may have a significant impact on radiation characteristics and the accuracy of experimental observations. As a result, precise modeling of ISR employing particle shower methods is critical for effectively interpreting experimental data and verifying theoretical predictions.

3.2. FSR

The emission of surplus radiation by departing particles in high-energy particle collisions is referred to as final-state radiation. The final state of radiation created in proton-proton collisions at the LHC can release further radiation before they are detected by the experimental instrument. This surplus radiation can carry away energy and momentum from the final state of radiation, influencing the characteristics of the observed radiation.

The alteration of the energy and momentum of the final state of radiation is one of the fundamental impacts of FSR. Because some of the energy is taken away by the released radiation, the emission of FSR can induce a decrease in the energy of the final state of radiation. This effect is particularly crucial for determining the masses of particles created in the collision. The alteration of the angular distribution of the final-state particles is another key impact of FSR. The emission of FSR particles might induce a departure from the predicted angular distribution of the final-state particles, affecting the accuracy of measurements of parameters such as particle spin produced in the collision. This makes FSR a crucial factor to consider in high-energy particle collisions because it may have an impact on particle characteristics and the accuracy of experimental observations.

3.2.1. Hard Interaction Radiation. The emission of high-energy radiation that is well-separated from the main jet. Hard radiation can arise from a variety of sources, including the emission of high-energy photons, at the point of the collision, or the production of heavy particles, such as W or Z bosons, in the collision. These represent a complex interplay of interactions at play, and their properties are crucial in understanding the underlying physics of the collision. By studying their behavior, scientists can gain a deeper understanding of the behavior of particles produced in high-energy collisions, leading to exciting developments. The study of hard radiation is an important topic in high-energy physics, as it can provide valuable information about the properties of the particles involved in high-energy particle collisions.

Theoretical calculations and Monte Carlo event generators are essential tools for accurately modelling hard radiation and understanding its effects on experimental measurements.

4. Jet Formation

The jets created at hadron colliders are clustered using Sequential Recombination Algorithms(SRAs). These SRAs influence the properties of the jets formed but, they are chosen on the bases of the physics question of interest. The anti-k$_T$ [5] algorithm is a sequential recombination jet algorithm that is infrared and collinear-safe by construction. It is one of the three most popular jet algorithms used in high-energy physics experiments along with the k$_T$ and Cambridge/Aachen algorithms. The kt algorithm is well-suited for identifying jets with soft radiation while the anti-k$_T$ algorithm is well-suited for identifying jets with hard radiation. The Cambridge/Aachen algorithm is less sensitive to soft radiation than the $_T$ algorithm. Due to their irrefutable utility in orchestrating the formation of jets to bring out the correct features of jets has made these algorithms a great focus of study in high-energy physics experiments. For our study, we used the anti-k$_T$ algorithm, which employs the following mathematical equation,

$$anti-k_T: \quad d_{ij} = \frac{1}{\max\left[p_{Ti}^2, p_{Tj}^2\right]} \frac{R_{ij}^2}{R_0^2}, \quad d_{iB} = \frac{1}{p_{Ti}^2},$$

R is the radius parameter.

5. Grooming Techniques

Grooming procedures are employed to eliminate pollution and increase the fidelity and clarity of the jet, allowing physicists to more correctly examine the underlying physics processes. Jet grooming procedures remove or reduce the effects of various causes of distortion on jets. They intend to separate the jet’s hardcore structure, which carries insights into the various physics involved. Numerous grooming procedures are utilized, each of which takes a distinct approach in eliminating contaminants from the jet.

Jet grooming strategies typically entail applying some criteria or conditions to the jet components or branches in order to choose which ones to preserve or discard. For example, one may eliminate the jet’s softest or most massive branches, or preserve just those that are a considerable mass drop or energy fraction relative to the parent jet, by employing different techniques. Jet grooming procedures can be used to increase the precision and reliability of jet observations and analysis. For example, jets emitted by heavy particles such as top quarks or vector bosons with distinguishing substructure properties such as two or three topics can be better identified. Jet grooming can potentially increase sensitivity to new physics processes that result in distinctive jet shapes or masses.

Trimming is one of the most common grooming procedures that involve re-clustering the jet with a smaller radius parameter and then deleting any subjets with a lower transverse momentum below a predetermined threshold. Pruning is another popular grooming procedure that eliminates particles from a jet that are not part of a hard substructure, such as soft radiation or the underlying event. Soft drop is another grooming technique that declutters a jet into sub-jets and eliminates soft radiation repeatedly until a specific condition is fulfilled, such as a minimum transverse momentum or a maximum angular spacing between sub-jets.

6. Results

In This paper, we have utilized the superior matrix element generation capability of Madgrapgh5(MG5) [6] compared to what standalone Pythia8(P8) [7] provides. Here MG5 can help in the simulation of much more realistic showers, with the help of P8, as MG5 can simulate one parton each incoming from each colliding proton going to up to four outgoing partons. Whereas P8 can only simulate up to two outgoing partons. The P8 hidden valley module is used for showering the dark matter model, and the utilized physical parameters are given in Table 1. The jet merging parameters are specified in Table 2.

Table 1. Set of physical parameters used in P8 hidden valley module.

Physical Parameters	Values
Ngauge	2
nFlav	1
alphaOrder	1
Lambda	6.5
pTminFSR	1.1
spinFv	0
FSR	On
fragmentation	On
probVector	0

Table 2. Set of Jet Matching parameters used in P8.

Jet Matching Parameters	Values
nJetMax	2
coneRadius	0.4
etaJetMax	10
qCut	100
nQmatch	5
clFact	1

The three main processes taking place are: Pair production of the dark matter candidate(χ),

$$pp \rightarrow \chi\bar{\chi},$$

Pair production of the bi-fundamental mediator(Φ)

$$pp \rightarrow \Phi\Phi^{\star},$$

Where the mediator further decays into the dark matter candidate and a jet(j)

$$\Phi \rightarrow \chi j,$$

Production of the bi-fundamental mediator and dark matter candidate,

$$pp \rightarrow \Phi\bar{\chi},$$

Where the mediator further decays into the dark matter candidate and a jet,

$$\Phi \rightarrow \chi j,$$

Handling of the data that comes from these generators for the purpose of managing jets is achieved through the software FastJet [8], which comes packed with the data analysis tool of our choice Rivet [9]. Rivet has been chosen as it provides a convenient infrastructure for adding our own analyses and allows the isolation and probing of specific types of events resulting in the accuracy and reliability of scientific results.

7. Event Selection

For the study of the observables, we have chosen trimmed fat jets of radius 1.0 with at least 250 GeV transverse momentum (p_T). These fat jets are constructed using the anti-$_T$ algorithm and trimming using the predetermined parameters, R_{sub} = 0.2 and f_{cut} = 0.05.

For signal probing, the fat jet and the MET's azimuthal separation should not be more than 1.0 radians, and should not be less than 1.0 radians for the background signal(BG). The signal jet is also called Semi-Visible Jets (SVJ) as a significant part of the jet goes undetected in the form of dark matter. The SVJ is chosen to be either the leading or sub-leading trimmed jet in p_T depending on which is closer to the MET. All the signal samples and BG samples, generated using MG5, at the center of mass energy of 13 TeV using the NNPDF2.3 LO PDF [10] set used with kt separation between partons of 100 GeV. The signals are generated by using a t-channel simplified dark-matter model [11] in MG5, The model has a mediator and dark-matter mass of 1500 GeV and 10 GeV, respectively. All BG signal samples generated solely using P8, are generated at 13 TeV, and with a minimum phase space cut of 500 GeV.

In Figure 1 all the events are BG processes, with MET being greater than 50 GeV for each event. Figure 2 and Figure 3 only include signal samples. Figure 4 compares two signal samples with one BG sample with MET has chosen to be above 200 GeV.

$$R_{inv} \equiv \left\langle \frac{\text{No. of Stable Dark Hadrons}}{\text{No. of Hadrons}} \right\rangle$$

Where, $R_{inv} \rightarrow 1$ corresponds to the generation of only stable dark hadrons resulting into MET, and $R_{inv} \rightarrow 0$ corresponds to a jet with all unstable dark hadrons that are decayed into the stable SM particles. Thus ideally a jet constructed with $R_{inv} \rightarrow 0$ should be as close as possible to a BG jet. Interestingly it is not the case what has been found and showed in the next section.

8. Results

Figure 1 shows that the absence of FSR (orange line) has a prominent effect on the substructure variable. Here both C_2 and LHA distributions shift toward the left when FSR is switched on, from which we can infer that more hard radiation corresponds to the FSR radiation as compared to ISR. The only significant effect of using the ME generation capabilities of MG5 is the distribution of MET. Also, it can be seen that MET and leading trimmed fat jets are mostly created in a "back to back" configuration and vice-versa for the sub-leading trimmed jet. From the thrust graph it can be seen that ISR and FSR don't have much of an effect but, using MG5 results in the domination of a significant number of multijet events over dijet events, though still having lesser multijet than configurations without MG5. This reflects an existence of the merging constraint and an inefficiency in the matching process when MG5 is showered with P8. τ_{32}^{WTA} tends to skew towards the right, suggesting the scarcity of three prong. This can be the contribution coming from the significant effect of the underlying event.

Graphs from Figure 2 study the signal samples and suggest, at extreme $\mathrm{R_{inv}}$ values corresponding to red and orange lines, shows an affinity of leading trimmed fat jets to be formed toward or away from the MET, respectively. For both $\mathrm{C_2}$ and LHA, the red line distribution is skewed towards the left and vice versa for the orange line. While the blue line and green line don't have much variation from each

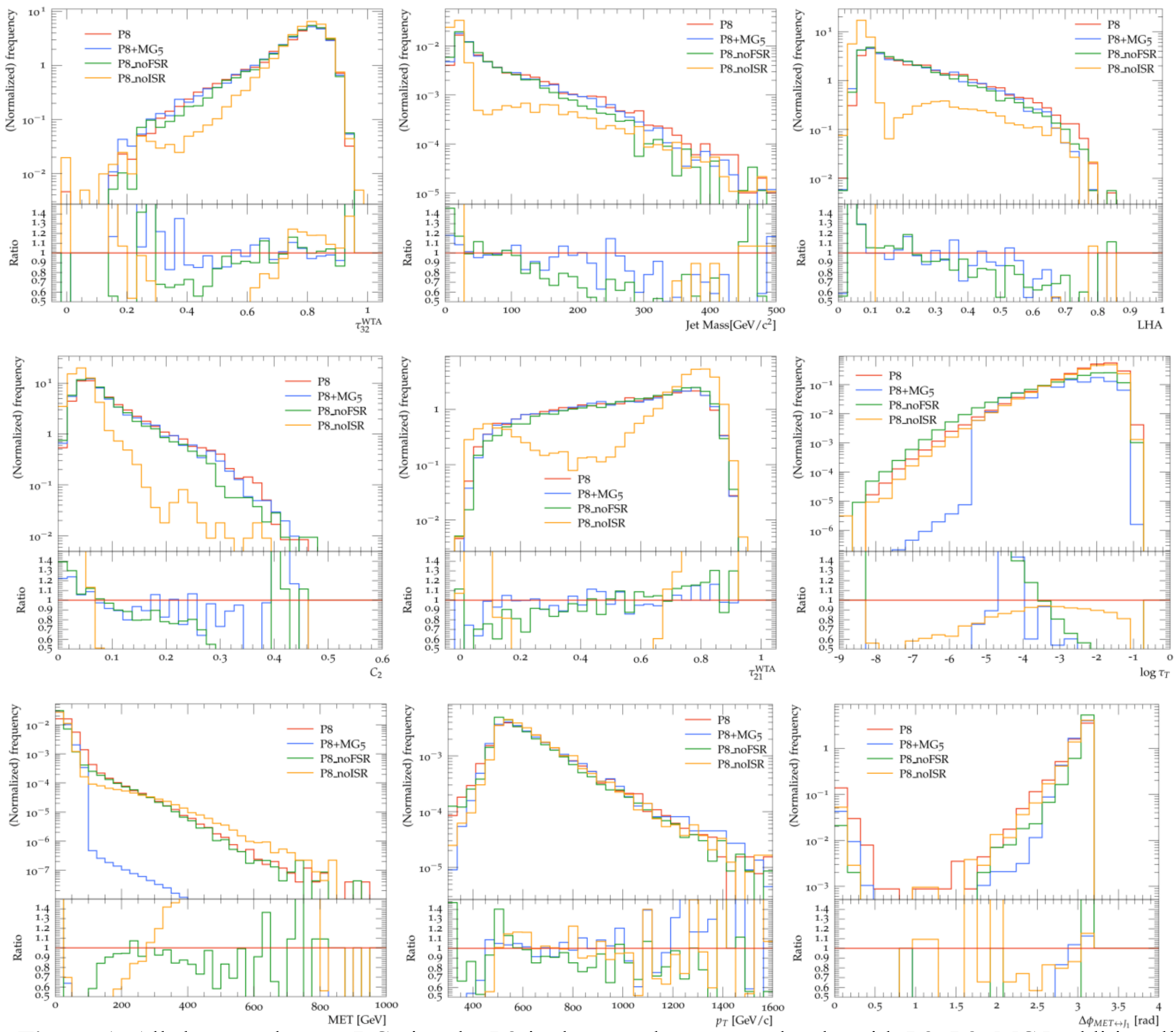

Figure 1. All the samples are BG signals. P8 is the sample generated only with P8, P8+MG5 additionally uses Madgraph5, P8_noFSR and P8_ noISR are the signals generated using only P8 with FSR and ISR switched ”off”,respectively.$\Delta\varphi_{MET} \leftrightarrow J_1$ shows the azimuthal difference between the MET and leading jet; MET distribution of all the events; log τT is the log of transverse thrust; p_T of the BG jet ; C_2 is the energy correlation function ; LHA is the Les Houches Angularity; $\tau^{WTA}{}_{21}$ and $\tau^{WTA}{}_{32}$ represent the N-subjettiness; Jet Mass is the mass of the BG jet.

other. Thus, we can conclude that there is a significant hard component contribution from the orange line and a soft component from the red line. τ_{32}^{WTA} distribution for the red line, towards 0 suggests a more multi prong structure, having lesser two prong structures as compared to the three prong one.

Figure 3 it can be seen that MET is Mostly in the direction of the sub-leading trimmed jet and in the opposite direction of the leading trimmed jet. Just like in the case of Figure 1, the absence of FSR (green

Journal of Physics: Conference Series **2663** (2023) 012052 doi:10.1088/1742-6596/2663/1/012052

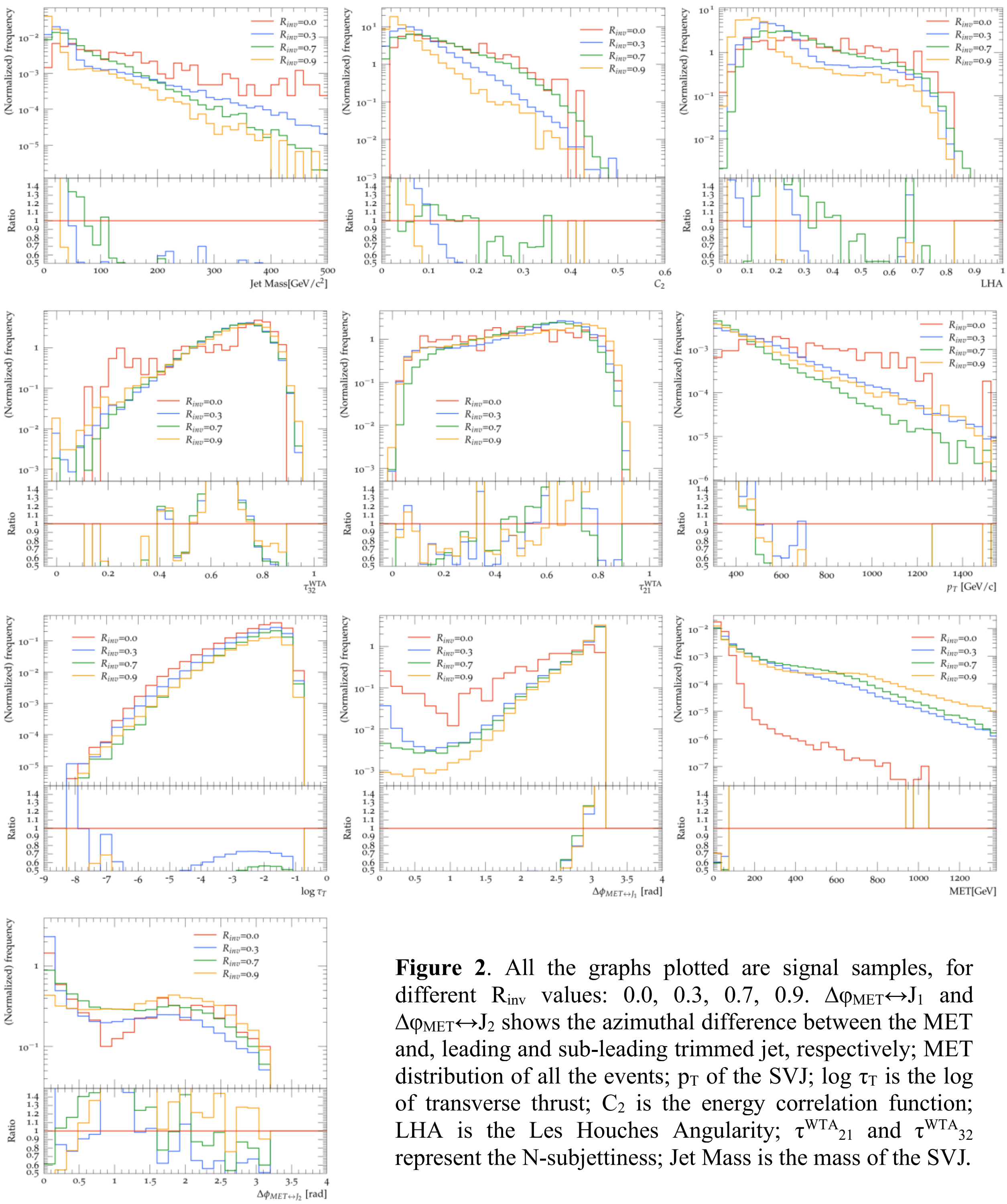

Figure 2. All the graphs plotted are signal samples, for different R_{inv} values: 0.0, 0.3, 0.7, 0.9. $\Delta\varphi_{MET}\leftrightarrow J_1$ and $\Delta\varphi_{MET}\leftrightarrow J_2$ shows the azimuthal difference between the MET and, leading and sub-leading trimmed jet, respectively; MET distribution of all the events; p_T of the SVJ; log τ_T is the log of transverse thrust; C_2 is the energy correlation function; LHA is the Les Houches Angularity; $\tau^{WTA}{}_{21}$ and $\tau^{WTA}{}_{32}$ represent the N-subjettiness; Jet Mass is the mass of the SVJ.

line) affects the substructure variables, C_2 and LHA, shifting their distributions toward the left, from which we can infer the non-abundance of hard radiation.

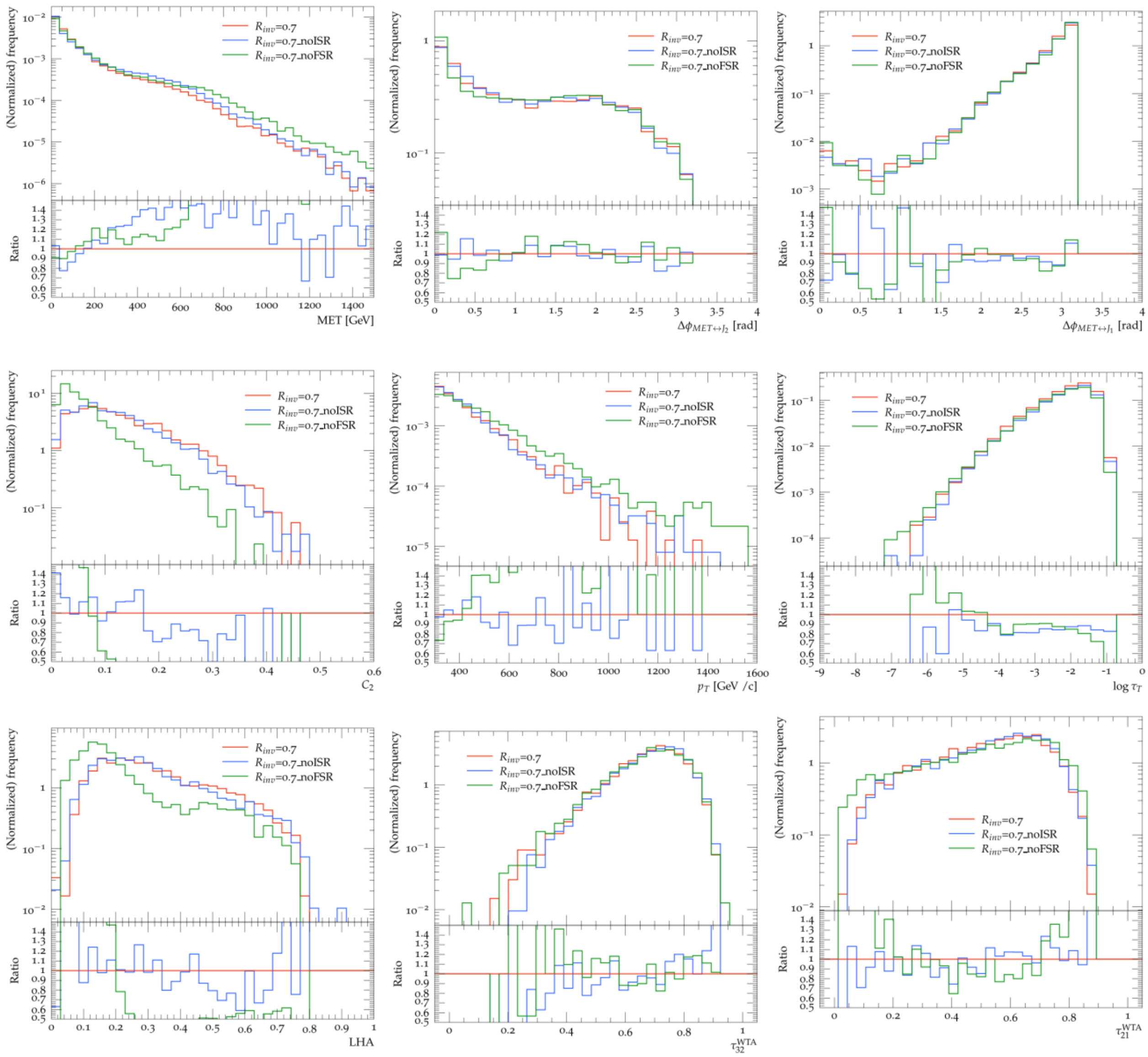

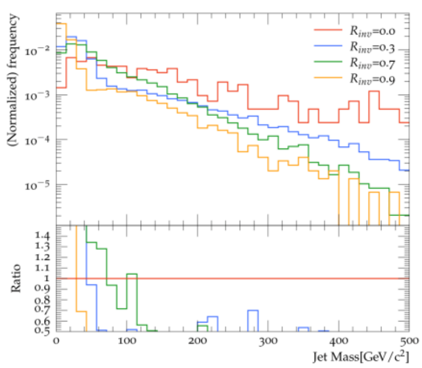

Figure 3. Graph compares signal samples for R_{inv} 0.7 with both FSR and ISR switched "on" and then each of them switched off individually. $\Delta\varphi_{MET} \leftrightarrow J_1$ and $\Delta\varphi_{MET} \leftrightarrow J_2$ show the azimuthal difference between the MET and, leading and sub-leading trimmed jet, respectively; p_T of the SVJ; log τ_T is the log of transverse thrust; C_2 is the energy correlation function; LHA is the Les Houches Angularity $\tau^{WTA}{}_{21}$ and $\tau^{WTA}{}_{32}$ represent the N-subjettiness; Jet Mass is the mass of the SVJ.

In Figure 4, the red and the blue lines correspond to the BG sample while the green line corresponds to a signal sample. The azimuthal distribution from the green and the red line, for the MET and the leading trimmed fat jet, suggests that the "back-to-back" configuration seems to be the dominant one

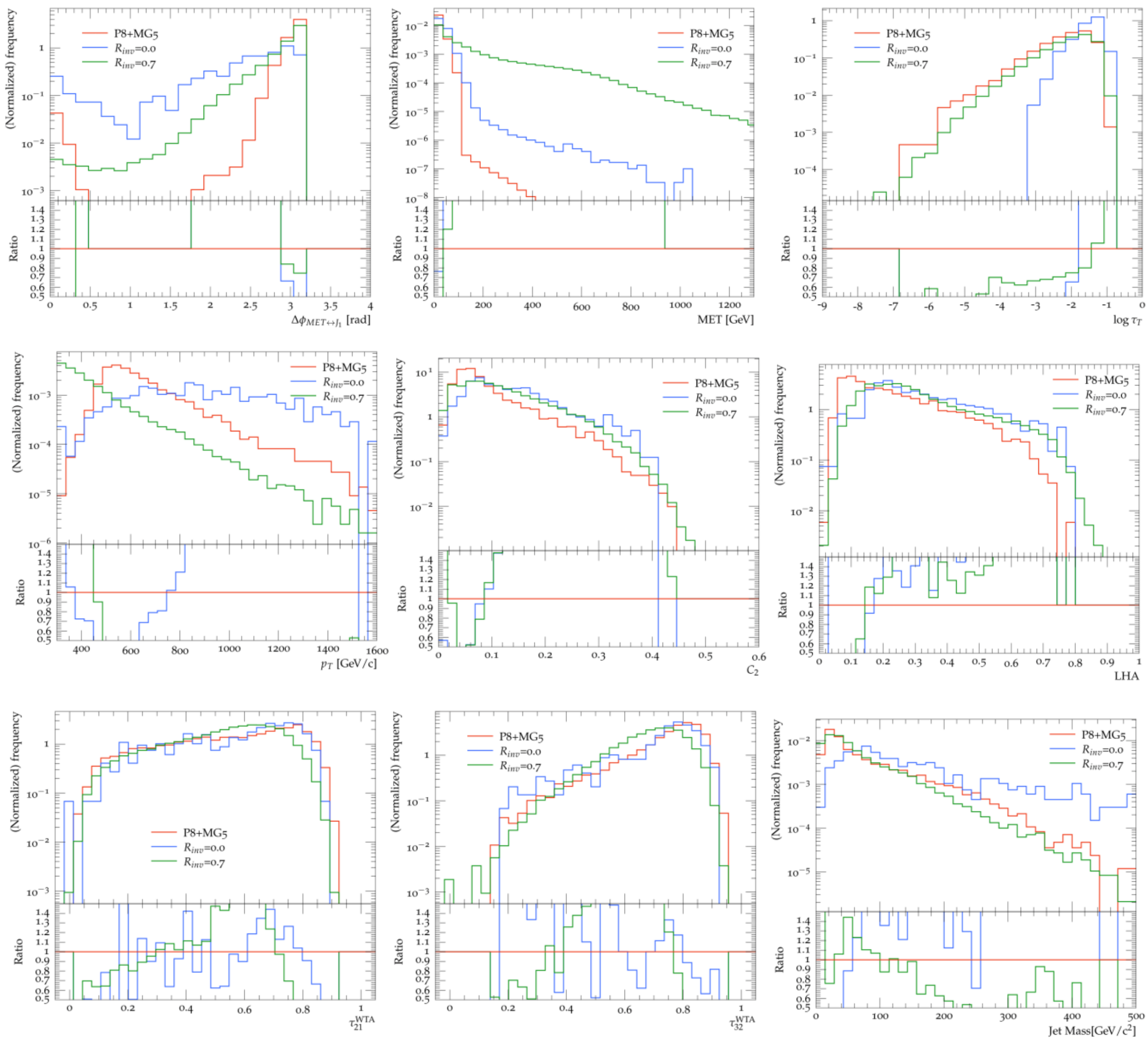

Figure 4. The graph compares the BG samples for the multi jet and R_{inv}= 0.0 events with signal sample R_{inv}= 0.7. $\Delta\varphi_{MET}\leftrightarrow J_1$ shows the azimuthal difference between the MET and leading trimmed jet; MET distribution of all the events; p_T of the SVJ; log τ_T is the log of transverse thrust; C_2 is the energy correlation function; LHA is the Les Houches Angularity; $\tau^{WTA}{}_{21}$ and $\tau^{WTA}{}_{32}$ represent the N-subjettiness; Jet Mass is the mass of the SVJ.

while for the blue line the azimuthal distribution seems to be less lopsided compared to others. Further, with the inclusion of MG5 with P8 (red line) there is an increase in dijet events while the blue line lacks dijet events. For C_2 The red line shifts to the left while the blue line shifts to the right telling us the red line has more soft components compared to the blue line. In a similar way, LHA also signals to the fact that the red line contains more soft components, than the other two. We can also infer that R_{inv}= 0.0 has a lesser number of low-mass jets and collectively jets with larger mass.

9. Conclusion

It can be inferred that different jet observables possess varying degrees of sensitivity toward changes in physics. For instance, τ_T exhibits significant sensitivity in distinguishing two jets from multi-jet radiations. Similarly, C_2 and LHA are sensitive to changes in the hard component of the radiation, as evidenced by their ability to probe in the presence or absence of final state and initial state radiations. In the context of dark matter searches, τ_{32}^{WTA} displays remarkable sensitivity in discriminating complex structures, while τ_{21}^{WTA} yield nothing noteworthy. Moreover, MET and Jet Mass for varying R_{inv} values also suggest the presence of undetected matter in the form of dark matter.

Acknowledgments
We would like to express our sincere gratitude to Amity University for providing us with outstanding infrastructure. We are also thankful to the Pythia8, Madgraph5, and Rivet experts for their valuable feedback and suggestions, which have helped us refine our methodology and enhance the quality of our research. Furthermore, we would like to acknowledge Dr. Deepak Kar for his exceptional guidance and mentorship on Pythia8. His deep knowledge of the subject and his willingness to share it with us have been invaluable. This project would not have been possible without the support, guidance, and contributions of all those mentioned above.

References

[1] Evans L and Bryant P 2008 *JINST* **3** S08001
[2] Gaillard M K, Grannis P D and Sciulli F J 1999 The Standard Model of Particle Physics *Rev. Mod. Phys.* 71 S96
[3] Roy D 2016 Proceedings of The European Physical Society Conference on High Energy Physics – PoS(EPS-HEP2015) (Austria)
[4] The ATLAS collaboration 2019 Measurement of jet-substructure observables in top quark, W boson and light jet production in proton-proton collisions at $\sqrt{s}$ = 13 TeV with the ATLAS detector. *J. High Energy Phys.* 08 033
[5] Cacciari M and Salam G P and Soyez G 2008 The anti-k_t jet clustering algorithm *J. High Energy Phys.* JHEP04(2008)063
[6] Alwall J *et al.* 2014 The automated computation of tree-level and next-to-leading order differential cross sections, and their matching to parton shower simulations *J. High Energy Phys.* JHEP07(2014)079
[7] Bierlich C *et al.* 2022 A comprehensive guide to the physics and usage of PYTHIA 8.3 *SciPost Phys. Codebases* 8 (*Preprint* 2203.11601)
[8] Cacciari M, Salam G P and Soyez G 2012 FastJet user manual *Eur. Phys. J. C* **72**
[9] Bierlich C *et al.* 2020 Robust independent validation of experiment and theory: Rivet version 3 *SciPost Phys.* **8** 026 (*Preprint* 1912.05451)
[10] Skands P, Carrazza S and Rojo J 2014 Tuning PYTHIA 8.1: the Monash 2013 tune *Eur. Phys. J. C* **74** 3024
[11] Cohen T, Lisanti M, Lou H K and Mishra-Sharma S 2017 LHC searches for dark sector showers *J. High Energy Phys.* JHEP11(2017)196